EDDY-CURRENT INVERSION OF FLAW DATA FROM FLAT-BOTTOMED HOLES

C. V. Dodd, J. R. Pate* and W. E. Deeds†

Metals and Ceramics Division
Oak Ridge National Laboratory
Oak Ridge, Tennessee 37831-6151

INTRODUCTION

The demands on our nondestructive evaluation techniques are increasing every year as our technical society becomes more and more complex. Rapid, accurate, and cheap inspection methods are needed to insure the safety, reliability, and economy of large power systems, transportation systems, and many gadgets on which our society has become dependent. Eddy-current tests have the required speed and the potential for the required accuracy and low cost. However, because of their complex nature, it has been costly to design these tests and interpret the data. To design more sensitive tests we need to be able to accurately compute the change in the eddy-current signal caused by a defect (the "forward" problem) in the presence of all of the other properties in the test. Then, to evaluate the data from the test we need to compute the defect size and location from the change in the eddy-current signal (the "inverse" problem) in the presence of the other property variations.

Various techniques have been applied to the solution of the forward problem over the years, with varying degrees of success. These solutions range from finite-element calculations to closed form integral equations. These techniques have been extremely helpful in the design of eddy-current tests that have a large number of properties varying at the same time (multiple-property tests). We can determine the best combination of coil and test operating parameters for the optimum detection of small defects in the presence of multiple-property variations.

The inverse calculation is based on the forward calculation so that, the better the forward calculations agree with the actual measurements, the better our inversion will be. Accurate inversion techniques will automatically detect, locate, and size defects as the probe is scanning past them. This will reduce the time for eddy-current inspections, eliminate the costly data interpretation, and remove any bias from the results.

GENERAL INVERSION TECHNIQUE

Our flaw inversion formulae are based on previous analytical solutions [1,2,3] to eddy-current problems and the infinitesimal flaw theory of Burrows [4]. We start with a pancake coil above a semi-infinite

*Intern Research Participant, Hendrix College.
†Adjunct Research Participant, The University of Tennessee, Knoxville.

plane, as shown in Fig. 1. The normalized impedance change, Z_{nd}, produced in a coil above a semi-infinite plane conductor by a defect with normalized volume Vol_n located at cylindrical coordinates r,z can be written as

$$Z_{nd}(r,z) = \frac{-3(\omega\mu\sigma\bar{r}^2)}{2\pi I_{air}} Vol_n \left[\int_0^\infty \frac{J(r_2,r_1)\ J_1(\alpha r)(e^{-\alpha\ell_1} - e^{-\alpha\ell_2})\ F(\alpha,\alpha_1,z)}{\alpha^3}\, d\alpha \right]^2 \quad (1)$$

where $$F(\alpha,\alpha_1,z) = \frac{\alpha e^{\alpha_1 z}}{\alpha + \alpha_1} \quad (2)$$

ω is the angular frequency of the eddy currents, and $J(r_2,r_1)$ is the integral of $xJ_1(x)$ with respect to x from αr_1 to αr_2. The normalized inner and outer radii of the coil are r_1 and r_2. The coil has mean radius $\bar{r} = (r_1+r_2)/2$ and is located at heights between ℓ_1 and ℓ_2 above the conductor, which occupies the region of negative z. The conductor has permeability μ, conductivity σ and a complex parameter $\alpha_1 = (\alpha^2+i\omega\mu\sigma\bar{r}^2)^{1/2}$. The term I_{air} is the integral evaluated for the coil in air. If we take the square root of both sides of Eq. (1), multiply the result by $rJ_1(ar)$, and integrate with respect to r from 0 to infinity, we have

$$\int_0^\infty rJ_1(ar)\ \sqrt{-Z_{nd}(r,z)}\ dr =$$

$$\left[\frac{3\omega\mu\sigma\bar{r}^2}{2\pi I_{air}} Vol_n \right]^{1/2} \int_0^\infty rJ_1(ar)dr \int_0^\infty \frac{J(r_2,r_1)J_1(\alpha r)(e^{-\alpha\ell_1} - e^{-\alpha\ell_2})F(\alpha,\alpha_1,z)}{\alpha^3}\, d\alpha \quad (3)$$

We can reduce the righthand side of the equation by use of the Fourier-Bessel integral, which is

$$f(a) = \int_0^\infty rJ_1(ar) \int_0^\infty \alpha J_1(\alpha r) f(\alpha)\ d\alpha\ dr \quad (4)$$

Eq. (3) then reduces to:

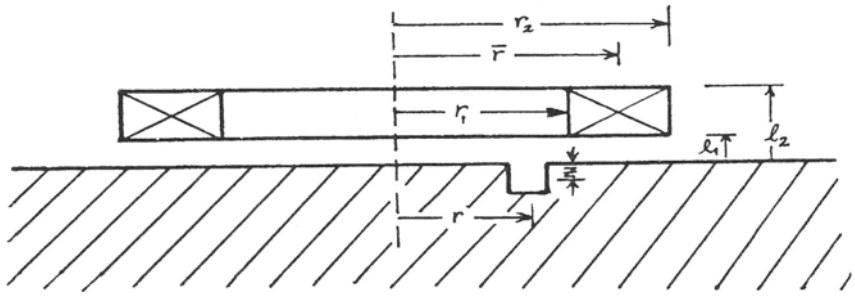

Fig. 1. Pancake coil above a semi-infinite conducting plane.

$$\int_0^\infty rJ_1(ar)\sqrt{-Z_{nd}(r,z)}\,dr = \left[\frac{3\omega\mu\sigma\bar{r}^2}{2\pi I_{air}}\,\mathrm{Vol}_n\right]^{1/2}\frac{J(r_2,r_1)(e^{-a\ell_1}-e^{-a\ell_2})^2F(a,a_1,z)}{a^3} \quad (5)$$

We can solve this equation directly for the depth of the defect, z, and the volume of the defect, Vol_n. If we let $x = \mathrm{Re}(a_1)$ and $y = \mathrm{Im}(a_1)$, and if we let

$$\sqrt{\mathrm{Vol}_n}\,e^{a_1 z} = CM_0 e^{i\theta} \quad (6)$$

where

$$C = \sqrt{\frac{2\pi I_{air}}{3\omega\mu\sigma\bar{r}^2}}\;\frac{a^3}{J(r_2,r_1)[\exp(-a\ell_1)-\exp(-a\ell_2)]} \quad (7)$$

$$M_0 = \mathrm{Mag}\left[(a+a_1)\int_0^\infty \sqrt{-Z_{nd}(r,z)}\,rJ_1(ar)\,dr\right] \quad (8)$$

and

$$\theta = \mathrm{Pha}\left[(a+a_1)\int_0^\infty \sqrt{-Z_{nd}(r,z)}\,rJ_1(ar)\,dr\right] \quad (9)$$

then $z = \theta/y$ (10)

and $\mathrm{Vol}_n = [CM_0\exp(-x\theta/y)]^2$ (11)

The pancake coil above a conducting semi-infinite plane is the simplest case and is the only one that we have been able to completely invert in an analytical form thus far. However, we are still able to solve the messier but more practical cases using numerical techniques. These cases include the pancake coil above any number of layers of conductors and coils encircling or in the bore of concentric cylindrical conductors. The case that has received the most study thus far is the pancake coil above a conducting plane of thickness c. The equation for the impedance change for the conducting plate is the same as Eq. (1) except that the function in Eq. (2) now becomes

$$F(\alpha,\alpha_1,z) = \frac{\alpha(\alpha_1+\alpha)e^{2\alpha_1 c}e^{\alpha_1 z} + \alpha(\alpha_1-\alpha)e^{-\alpha_1 z}}{-(\alpha-\alpha_1)^2 + (\alpha_1+\alpha)^2 e^{2\alpha_1 c}} \quad (12)$$

This equation is based on the assumption that the defect is small with respect to the coil and with respect to variations in the eddy-current field (vector potential) generated by the coil. In most practical eddy-current tests this will not be the case. An eddy-current test would be relatively insensitive to a defect small enough to meet these criteria. However, we can use these equations to design optimum tests for very small defects and assume the designs will be good if not exact for the larger defects. Since the accuracy of inversion depends on the accuracy of the forward calculations, we will first look at different forward calculations and the experimental measurements.

FORWARD PROBLEM

The forward problem was calculated using three different methods. The first used the small defect approximation, as shown in Eq. (1) and Eq. (12), with r and z being at the center of the defect. Next we averaged the defect signal over the depth of the defect by computing Eq. (1) at the different values of z. Finally, we averaged the defect signal over the volume of the defect, by computing Eq. (1) at different values of r and z throughout the volume of the defect. None of these approximations is really correct. The individual volume elements cannot be summed as we have done, since there is an interaction term between the different volume elements that is being neglected. These terms can have a very significant contribution, particularly for large defects. We used experimental measurements to guide us in determining how much improvement each technique would give.

For the experimental measurements, we used a pancake coil on an aluminum plate. The pancake coil had a mean radius $\bar{r} = 6.5$ mm and was optimized to detect defects in the 6.4-mm-thick plate. The measurements were made with a Zetec MIZ-17 eddy-current instrument at a frequency of 500 Hz. This instrument gave voltages that were proportional to the real and imaginary parts of the impedance. We measured the magnitude and phase shift caused by a known amount of probe lift-off. We used this magnitude and phase to compute the gain and phase shift needed to normalize the impedance. Each side of the plate had six flat-bottomed holes machined to depths of approximately 90, 75, 60, 50, 40 and 30% of the wall. The diameter of each hole is approximately equal to its depth. The plate was scanned by a precision XYZ scanner controlled by a PC-AT clone over the IEEE-488 bus. The voltages measured from the MIZ-17 were digitized and also sent to the computer over the bus.

A composite of the three different methods of computing the normalized impedance change along with the measured impedance change for a 90% near-side defect is shown in Fig. 2. The single-point defect calculation (SPT) is poor, the average over depth (DEP) is better, and the average over volume (VOL) is the best. However, none of the calculated impedances agree very well with the experimental. Since the measurements for the 60% far-side defect, we get considerably better agreement between all the calculations and the measurement, as shown in Fig. 3. Note that now the measurement noise has increased considerably. We are approaching the limit of accurate defect measurements for this particular combination of probe and conductor geometry, although other eddy-current methods allow the accurate sizing of the 30% far-side defect. We shall now see how these defect signals can be inverted.

INVERSE PROBLEM

The inversion of the normalized impedance change for a pancake coil above a conducting plate [Eqs. (1) and (12)] can be done in a manner similar to the inversion of the coil above a semi-infinite plate. The application of the Fourier-Bessel integral gives the same results as Eq. (5) but with the more complicated expression for $F(a,a_1,z)$. We have

$$\int_0^\infty rJ_1(ar)\sqrt{-Z_{nd}(r,z)}\,dr = \left[\frac{3\omega\mu\sigma\bar{r}^2}{2\pi I_{air}}\,\mathrm{Vol}_n\right]^{1/2}\frac{J(r_2,r_1)(e^{-a\ell_1}-e^{-a\ell_2})F(a,a_1,z)}{a^3} \tag{13}$$

where

$$F(a,a_1,z) = \frac{a(a_1+a)e^{2a_1c}e^{a_1z} + a(a_1-a)e^{-a_1z}}{-(a-a_1)^2 + (a_1+a)^2 e^{2a_1c}} \tag{14}$$

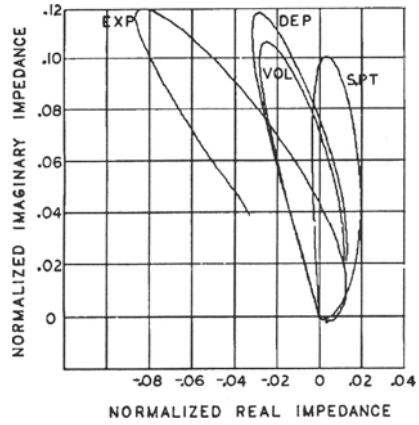

Fig. 2. Normalized impedance change due to a 90% near-side defect.

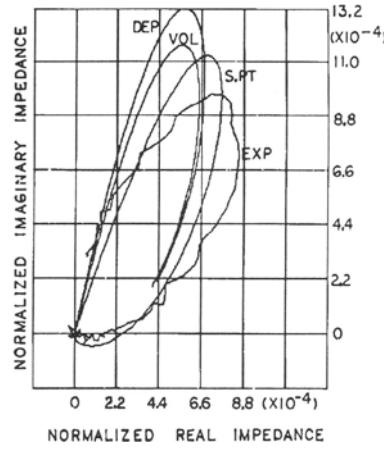

Fig. 3. Normalized impedance change due to a 60% far-side flat bottom hole.

While this expression prevents us from solving the equation directly we can vary the defect depth z until the phase on the righthand side matches the phase on the lefthand side of the equation. The same technique can be used for the averages over the depths and over the volume, but we shall save those for later. In Fig. 4 we show how the scan over the defect signal contributes to the calculation of the depth (DEP) and volume (VOL) of the defect as the probe is scanned in the r direction. The defect magnitude (shown as MAG on the figure) and phase are calculated. The depth and volume obtained by evaluation of Eq. (13) agree quite well with the initial depth and volume, as we would expect if our program were correct. What is missing is some "real world noise." When this is added, the results deteriorate considerably. The reason is that the integral has a large contribution from regions where the coil is measuring mostly noise. The solution is to make a window around our sensitive region so that the integral contribution comes from values of r that have high signal-to-noise ratios.

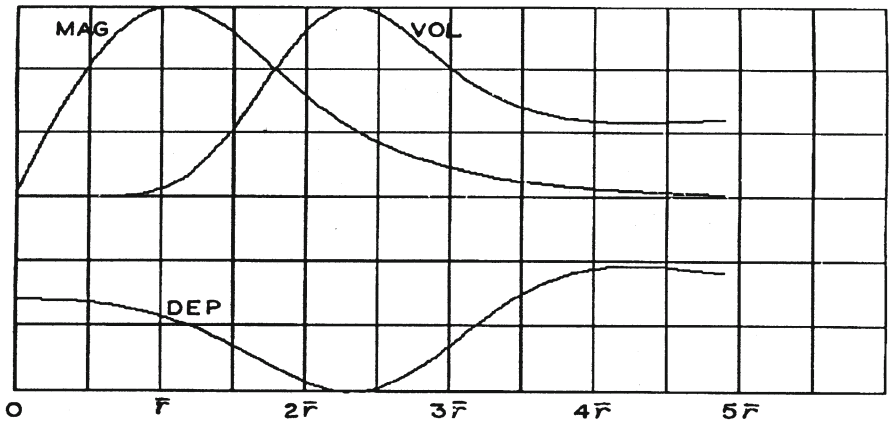

Fig. 4. Defect inversion calculation and the contributing factors plotted against flaw radial position.

WEIGHTING FUNCTIONS

For eddy-current measurements this will be the region directly under the coil, as we can see for the large magnitude of $Z_{nd}(r,z)$. We have chosen the values of r_1 and r_2 although this is somewhat arbitrary. The constant a in the Fourier-Bessel equation [Eq. (4)] can have any value, and we can sum over these values on both sides of Eq. (13). In addition, each of the different Bessel functions can be multiplied by a constant. The constants can be selected so that the result is most sensitive to the region directly below the coil. Finally, the constants may be determined by using the orthogonality properties of the Bessel functions. This was done for a 20-term polynomial weighting function that we choose to be unity between r_1 and r_2 and zero elsewhere. This gave an approximate square wave, but it had a lot of ringing. This approximation is probably good enough for most of our eddy-current calculations, and the results obtained from experimental data were as good as our better weighting functions. However, it is somewhat cumbersome to use when inverting actual eddy-current readings in real time. We therefore improved our weighting function by letting the number of terms approach infinity. The equation for the weighting function then becomes the Fourier-Bessel function, given in Eq. (4). The weighting function becomes an actual square wave. We can therefore replace the lefthand side of Eq. (13) by a square wave and perform the integration on the righthand side and get

$$\int_{r_1}^{r_2} \sqrt{-Z_{nd}(r,z)}\, dr = \tag{15}$$

$$\left[\frac{3\omega\mu\sigma\bar{r}^2}{2\pi I_{air}}\,\mathrm{Vol}_n\right]^{1/2} \int_0^{\infty} \frac{J(r_2,r_1)[J_0(ar_1) - J_0(ar_2)](e^{-al_1} - e^{-al_2})F(a,a_1,z)}{a^4}\, da$$

We show a comparison of the defect size and depth calculated using the 20-term weighting function and the infinite term weighting function in Table 1 (near side) and Table 2 (far side). The equations are evaluated using both computed data and experimental data. The two different weighting functions give essentially the same results, so either could be used. Although the initial calculations for the infinite term weighting function would require longer initial calculations for the depth and volume [the evaluation of the righthand side of Eq. (15)], these values could be stored in a look-up table in memory. The lefthand side of the equation can be calculated very rapidly as the plate is being scanned. The agreement is poor for large, near-side defects. The

Table 1. Calculated and experimental inversion for near-side defects

	Calculated			Experimental		
	Actual	Twenty Term	Infinite Term	Twenty Term	Infinite Term	Corrected Value
Depth	-0.4343	-0.4345	-0.4342	-0.1622	-0.1630	-0.3941
Volume	0.5147	0.5150	0.5143	0.2778	0.2789	0.4904
Depth	-0.3688	-0.3690	-0.3688	-0.1612	-0.1613	-0.3879
Volume	0.3152	0.3154	0.3150	0.1970	0.1971	0.3357
Depth	-0.3078	-0.3080	-0.3078	-0.1483	-0.1484	-0.3409
Volume	0.1856	0.1857	0.1855	0.1304	0.1306	0.2100
Depth	-0.2510	-0.2511	-0.2509	-0.1205	-0.1202	-0.2380
Volume	0.1017	0.1017	0.1016	0.0746	0.0744	0.1036
Depth	-0.1882	-0.1883	-0.1882	-0.1076	-0.1071	-0.1903
Volume	0.0428	0.0428	0.0428	0.0389	0.0379	0.0366
Depth	-0.1529	-0.1530	-0.1529	-0.0958	-0.0965	-0.1517
Volume	0.0216	0.0216	0.0216	0.0223	0.0223	0.0052

agreement becomes much better for far-side defects. The agreement improves as the defect size decreases up to a point, and then the defect is lost in the noise. This is approximately the same way the agreement between the calculated and measured forward calculations vary. While the example shown is for the most simple forward calculation and inversion, it can be done in a similar manner for the averaging methods also. It is important to note that, while the exact agreement is poor, a correction formula can be easily obtained that relates defect depth to the value obtained from inversion. The last column in both tables, labeled "Corrected Value," shows a linear least-squares fit of the experimental inverted value to the actual depth and volume values. Due to the extreme nonlinearity of eddy-current responses, this is quite difficult to do with raw eddy-current data.

Table 2. Calculated and experimental inversion for far-side defects

	Calculated			Experimental		
	Actual	Twenty Term	Infinite Term	Twenty Term	Infinite Term	Corrected Value
Depth	-0.4333	-0.4331	-0.4334	-0.5976	-0.5989	-0.4411
Volume	0.5145	0.5148	0.5141	0.3439	0.3426	0.4255
Depth	-0.3686	-0.3683	-0.3687	-0.3759	-0.3773	-0.3539
Volume	0.3171	0.3173	0.3168	0.3277	0.3263	0.3989
Depth	-0.3059	-0.3055	-0.3060	-0.2533	-0.2537	-0.3053
Volume	0.1845	0.1846	0.1843	0.2154	0.2153	0.2182
Depth	-0.2510	-0.2505	-0.2511	-0.1262	-0.1347	-0.2585
Volume	0.1010	0.1012	0.1010	0.1304	0.1276	0.0754
Depth	-0.1882	-0.1876	-0.1883			
Volume	0.0437	0.0438	0.0436			
Depth	-0.1529	-0.1521	-0.1531			
Volume	0.0219	0.0220	0.0219			

SUMMARY AND CONCLUSIONS

The results obtained to date show a good correlation between the computed and measured volume and depth of the defect. While this work is very promising, follow-on measurements should include additional frequencies and additional geometry and conductivity variations. Future work should also include empirical correction equations, defect interaction correction terms and more accurate inversion equations.

ACKNOWLEDGMENTS

Research was sponsored by the Office of Nuclear Regulatory Research, U.S. Nuclear Regulatory Commission under Interagency Agreement DOE 1886-8041-7B with the U.S. Department of Energy under Contract DE-AC05-84OR21400 with Martin Marietta Energy Systems, Inc.

REFERENCES

1. C. V. Dodd, W. E. Deeds, and J. W. Luquire, "Integral Solutions to Some Eddy-Current Problems," *Int. J. Nondestr. Test.* 1(1), 29-90 (June 1969).
2. C. C. Cheng. C. V. Dodd, and W. E. Deeds, "General Analysis of Probe Coils Near Stratified Conductor," *Int. J. Nondestr. Test.* 3(3), 109-130 (September 1971).
3. C. V. Dodd, C. C. Cheng, and W. E. Deeds, "Induction Coils Coaxial with an Arbitrary Number of Cylindrical Conductors," *J. Appl. Phys.* 45(2), 638-647 (February 1974).
4. M. L. Burrows, *A Theory of Eddy-Current Flaw Detection* (Ph.D. Dissertation), University of Michigan, Ann Arbor (1964).